Journal of Metals, Materials and Minerals, 35(3), e2308, 2025

Improving the mechanical performance of 45S5 3D scaffolds through the particles of barium titanate ceramics

Surirat YOTTHUAN[1,*], Usanee PANTULAP[1], Nuttawan SAWANGBOON[1], Ornuma TUNGSANGUAN[1], Ekarat MEECHOOWAS[1], Kansiree KAEWMORAKOT[1], Nathaporn UTHAICHAI[1], and Theerachai BONGKARN[2]

[1] *Department of Science Service, Ratchathewi, Bangkok 10400, Thailand*
[2] *Department of Physics, Faculty of Science, Naresuan University Phitsanulok 6500, Thailand*

***Corresponding author e-mail**: surirat@dss.go.th

Received date:
12 February 2025
Revised date:
19 March 2025
Accepted date:
10 June 2025

Keywords:
Bioactive glass;
Barium titanate;
Scaffold;
Bone regeneration

Abstract

Bioglass® 45S5 is widely used in bone tissue engineering due to its excellent bioactivity. However, its low mechanical strength remains a major limitation. In this study, 25 wt% barium titanate ($BaTiO_3$; BT) was incorporated into 45S5 scaffolds to improve mechanical performance and modulate bioactivity. The 3D scaffolds were fabricated using the foam replication method and exhibited interconnected porosity, with average pore sizes of 471 ± 94 μm (45S5) and 598 ± 58 μm (45S5/BT25), closely resembling human bone. The addition of BT increased the density and compressive strength of the scaffolds to 2.89 ± 0.18 g·cm^{-3} and 2.0 ± 0.2 MPa, respectively. Bioactivity evaluation in simulated body fluid (SBF) revealed delayed carbonated hydroxyapatite (CHA) formation in 45S5/BT25 scaffolds, with CHA detected after 21 days, compared to 7 days in pure 45S5. This delay was consistent with FTIR, SEM-EDS, and XRD results and is likely attributed the formation of a stable $Ba_2TiSi_2O_8$ phase. Overall, these results indicate that BT-modified 45S5 scaffolds not only exhibit improved mechanical performance but also offer tunable bioactivity, making them promising candidates for tailored bone regeneration applications.

1. Introduction

The increasing incidence of bone tissue damage caused by conditions such as osteoporosis, bone cancer, automobile accidents, aging-related degeneration, and other traumatic injuries highlights the urgent need for effective synthetic bone substitutes [1-3]. Among these, bio-ceramics have emerged as promising materials for both bone replacement and as porous matrixes for tissue engineering due to their superior bio-compatibility and ability to support bone regeneration [4]. In the late 1960s, Hench and Wilson introduced the first bioactive glass, Bioglass® 45S5, with a composition of 45% SiO_2, 24.5% CaO, 24.5% Na_2O, and 6% P_2O_5 by weight [5]. This material remains one of the most studied bioactive glasses due to its exceptional ability to bond with bone tissue and stimulate mineralization. The exceptional properties of 45S5 bioactive glass have made it a material of choice for orthopedic and dental applications, as well as for fabricating scaffolds in tissue engineering [6-9]. Despite these advantages, its poor mechanical strength limits its application in load-bearing bone repairs. This drawback necessitates the development of strategies to enhance its mechanical performance without compromising its bioactivity.

Various strategies have been explored to overcome the mechanical limitations of bioactive glasses. Piezoelectric materials have gained substantial attention in recent years for their potential to improve the mechanical properties of bioactive materials while also introducing beneficial electro-mechanical effects. Lead-free piezoelectric materials such as barium titanate ($BaTiO_3$, BT), potassium sodium niobate ($KNa_{0.5}Nb_{0.5}O_3$), and lithium sodium potassium niobate ($Li_{0.06}Na_{0.5}K_{0.44})NbO_3$ have emerged as viable candidates for improving both mechanical reinforcement and functional stimulation in bone-related applications [10-14]. In addition, these materials offer piezoelectric effects, which can promote bone regeneration by boosting cellular activity [10-12]. Among lead-free candidates, barium titanate (BT) stands out for its piezoelectric behavior, biocompatibility, and potential to reinforce bioactive matrices [10-12]. For instance, Saeidi *et al.* [10] used the freeze casting technique to fabricate piezoelectric composite scaffolds with 75% BT and 25% nanobioglass (nBG; 63 mol% SiO_2, 28 mol% CaO, 9 mol% P_2O_5). After sintering at 1250°C for 2 h, the resulting scaffolds exhibited improved density, mechanical strength, and piezoelectric constant (d_{33}). The scaffolds showed enhanced density, a d_{33} of ~25 pC/N and compressive strength (16.9 ± 1.1 MPa) in comparison to nBG scaffolds. The resulting d_{33} value was significantly higher than that of natural human bone (0.7 pC/N) [15], which could facilitate bone regeneration. These improvements surpass the properties of natural bone, highlighting the potential of BT for biomedical applications. Similarly, Polley *et al.* [11] and Zhang *et al.* [16] have both reported the remarkable mechanical improvements in BT-based composites, demonstrating compressive strengths far superior to those of undoped bioactive glasses. In order to create functional, 3D biomaterials for bone regeneration, Polley *et al.* [11] combined the benefits of piezoelectric BT and 45S5 (BT = 85 wt% and 45S5 = 15 wt%) using an additive manufacturing technique. The composite scaffolds were sintered at 1150°C for 1 h. Their composite scaffolds achieved an

impressive strength of 56.4 ± 7.6 MPa. Likewise, Zhang *et al.* [16] successfully fabricated highly porous HA/BT piezoelectric composite (containing 10 wt% hydroxyapatite (HA) and 90 wt% BT) with aligned lamellar porosity using an ice templating technique at sintering temperature of 1250°C for 3 h. The samples exhibited the highest compressive strength of 14.5 MPa and d_{33} of 2.8 pC/N, and the lowest porosity of 57.4%.

While BT-based composites have been widely studied, few have systematically investigated the direct incorporation of BT into the well-established 45S5 system using the foam replication technique. The use of this method to incorporate BT and create scaffolds with interconnected porosity that mimicked natural bone architecture has been rarely reported. This method ensures that the scaffolds exhibit high porosity, crucial for cell migration, nutrient diffusion, and vascularization [17,18]. Furthermore, limited studies have addressed how BT affects the phase evolution, densification behavior, pore structure, and time-dependent hydroxyapatite (HA) formation within 45S5 scaffolds. Moreover, the formation of secondary crystalline phases such as $Ba_2TiSi_2O_8$ and their potential role in modulating bioactivity remains underexplored. Addressing this gap is crucial for developing advanced composite materials that combine the bioactivity of 45S5 with the mechanical and piezoelectric benefits of BT.

This work aims to address these knowledge gaps by incorporating 25 wt% BT into 45S5 scaffolds using the foam replication method. The effects of BT addition on phase composition, microstructure, in vitro bioactivity, and mechanical properties are comprehensively evaluated. The novelty of this work lies in demonstrating the tunable bioactivity and enhanced mechanical strength in BT-modified 45S5 scaffolds, with delayed but sustained hydroxyapatite formation. This feature offers potential clinical relevance for applications requiring gradual osteointegration, such as in large or slowly healing bone defects. The findings will not only provide a deeper understanding of the material interactions and properties of 45S5/BT composites but also pave the way for the development of next-generation biomaterials that meet the demands of load-bearing applications. The insights gained from this research could have far-reaching implications for the design and fabrication of bioactive scaffolds, ultimately improving patient outcomes in orthopedic and dental treatments.

2. Experimental

2.1 Materials and sample preparation

The 45S5 scaffold was fabricated with the incorporation of 25 wt% barium titanate ($BaTiO_3$; BT), referred to as 45S5/BT25, using the foam replication technique. The raw materials included BT powder (99% purity, Thermo scientific, DE) and commercial 45S5 bioactive glass powders composed of 45 wt% SiO_2, 24.5 wt% CaO, 24.5 wt% Na_2O, and 6 wt% P_2O_5 (SCHOTT, DE). A 6% w/v solution of polyvinyl alcohol (PVA) (98% to 98.8%, Thermo scientific, USA) was prepared by dissolving PVA in deionized water at 80°C under stirring. The glass and ceramic powders were weighed according to the desired stoichiometry and mixed with the PVA binder solution using a magnetic stirrer at room temperature for 1 h to form a homogeneous slurry. Polyurethane (PU) foam templates (Eurofoam Deutschland GmbH Schaumstoffe, DE) were cut into cylindrical shapes with 12 mm diameter × 10 mm height (for compressive testing) and 12 mm diameter × 6 mm height (for bioactivity testing). The PU foam were immersed in the slurry for 1 min, dried at 60°C for 1 h, and the coating process was repeated three times to ensure uniform coverage. The coated foams were subjected to a two-step sintering process: first, at 400°C for 1 h to remove the PU foam and binder, and subsequently at 1000°C for 2 h in air to sinter the scaffold, using a Carbolite CWF 1100 furnace (UK). The heating and cooling rates were set at 2 °C·min^{-1} and 5°C·min^{-1}, respectively. To evaluate in vitro bioactivity, the sintered scaffolds were immersed in simulated body fluid (SBF). The SBF was prepared by dissolving reagent-grade chemicals including NaCl (99.5%, Carlo erba, IT), $NaHCO_3$ (99.5%, Supelco, DE), KCl (99.5%, Sigma-Aldrich, DE), $K_2HPO_4 \cdot 3H_2O$ (99%, Sigma-Aldrich, DE), $MgCl \cdot 6H_2O$ (98%, Sigma-Aldrich, DE), HCl (Carlo erba, IT) and $CaCl_2$ (95%, Supelco, DE) in distilled water. The solution was buffered to pH 7.4 using 1 M HCl and maintained at 37°C. The scaffolds were placed in an incubator (Patek OM15/OM15C) shaken at 90 rpm at 37°C for 7 days, 14 days, and 21 days. The pH of the SBF was monitored throughout the immersion period. After immersion, the samples were gently rinsed with distilled water and dried at 60°C for 12 h in a BINDER FED 53 drying oven (DE).

2.2 Characterizations

2.2.1 Phase evolution

X-ray diffraction (XRD, Bruker, D8 Advance, DE) was used to identify the phase structures in powdered scaffold samples. The XRD measurements were carried out using Cu-Kα radiation (λ=1.540 Å) operated at 40 kV and 35 mA. XRD patterns were recorded over a 2θ ranging of 10° to 60° with a step size of 0.02° at a scan speed of 1°·min^{-1}.

2.2.2 Microstructural characterization

Surface morphologies and elemental compositions of the samples were observed by scanning electron microscopy (SEM) with energy-dispersive X-ray spectroscopy (EDS) (JEOL, JSM-6610LV, JP) operated at an accelerating voltage of 20 kV. Prior to observation, the samples were sputter-coated with gold using a Quorum Technologies, Q150R ES Plus instrument (UK).

2.2.3 Density measurement

The density (ρ) of sintered scaffold was measured by the Archimedes technique using distilled water (DI) as the immersion medium (Sartorius, BP 210D, DE). Three samples from each composition were used for measurement. The density was calculated using the following Equation below:

$$\rho = \frac{W(a)}{W(a) - W(l)} * \rho_{(DI\ water)}$$

Where $W(a)$ is weight of the sample in air, $W(l)$ is weight of the sample immersed in liquid, and ρ(DI water) is density of DI water at room temperature.

2.2.4 FTIR analysis

Fourier Transform Infrared Spectroscopy (FTIR, Bruker Tensor 27, DE) was used to examine structural changes and hydroxyapatite (HA) formation before and after immersion in SBF. Spectra were collected in the absorbance mode using the KBr pellet method, within the wavenumber range of 400 cm^{-1} to 2200 cm^{-1} and a spectral resolution of 0.5 cm^{-1}. All measurements were performed in triplicate to ensure reproducibility.

2.2.5 Mechanical analysis

Compressive strength tests were carried out using a universal testing machine (Instron Electropuls E10000, UK). Cylindrical scaffold samples (12 mm diameter × 10 mm height) were tested in uniaxial compression mode at a crosshead speed of 0.5 mm·min^{-1} under ambient conditions. The mean value and standard deviation were calculated from three replicate measurements for each sample group.

2.2.6 Statistical analysis

All quantitative experiments were performed in triplicate (n=3) for each composition. Results for density, compressive strength, and weight loss (%) are presented as mean ± standard deviation (SD). Pore size analysis was conducted using 20 representative SEM images per sample, and pore diameters were measured using ScopePhoto software. Statistical comparisons were analyzed using OriginPro (OriginLab Corp., USA), and significance was evaluated at $p < 0.05$.

3. Result and discussion

Figure 1(a-b) displays the XRD patterns at room temperature, in the 2θ range of 10° to 60°, for the 45S5 and 45S5/BT25 composite scaffolds before and after 0 day, 7 days, 14 days, and 21 days immersion in SBF. Before soaking, the 45S5 scaffold exhibited the $Na_6Ca_3Si_6O_{18}$ (JCPDS file no 01-077-2189). After immersion in SBF, peaks corresponding to hydroxyapatite phases [HA, $Ca_5(PO_4)_3(OH)$, JCPDS file no 00-009-0432] became progressively visible, indicating HA formation over time (Figure 1(a)). In contrast, the 45S5/BT25 composite scaffolds showed a predominant crystalline phase $Ba_2TiSi_2O_8$ (JCPDS file no 00-022-0513) alongside two minority phases $Na_6Ca_3Si_6O_{18}$ and $BaTiO_3$ (Figure 1(b)). The diffraction peak patterns of BT pure powder showed single peak around 39° and dual peaks around 45°, which is confirmed to be a tetragonal phase (JCPDS file no 01-071-0946). The $Na_6Ca_3Si_6O_{18}$ phase may have formed due to the crystallization of the 45S5 at elevated temperatures [11,19]. The development of this crystalline sodium-calcium-silicate phase contributed to the enhanced densification of the matrix [11,19]. The $Ba_2TiSi_2O_8$ phase remained stable throughout immersion, with increasing peak intensity over time (Figure 1(b)). This stability suggests that the BT addition induces a slower transformation to HA, as the formation of $Ba_2TiSi_2O_8$ hinders ion exchange and silica network dissolution, key processes in HA formation. This delay aligns with similar observations in BT-modified bioactive glasses, as reported by Polley *et al.* [11]. The presence of $Ba_2TiSi_2O_8$ likely results from the interaction between BT and 45S5 during sintering [11], where barium ions react with the silica network to form this stable phase.

FTIR analysis was carried out to further inspect the HA formation. The FTIR spectra of composite scaffolds after 0 day, 7 days, and 21 days of immersion in SBF were recorded, as shown in Figure 2(a-b). It is well known that the two bands at 566 cm^{-1} and 603 cm^{-1} correspond to the P-O bending vibrations in crystalline HA [20]. The band at 873 cm^{-1} and dual broad bands at 1417 cm^{-1} to 1487 cm^{-1} can be assigned to the stretching vibration of C-O bond [21], indicating that the formed HA was actually carbonated hydroxyapatite (CHA) [22]. These characteristic bands are not present in the spectra of 45S5 scaffolds before and 45S5/BT25 scaffolds before and after immersion for 7 days. While the 45S5 scaffolds after 7 days and 21 days and 45S5/BT25 scaffolds after 21 days of immersion in SBF indicate a clear CHA formation. The delayed onset of CHA formation compared to 45S5 scaffolds is consistent with the XRD results and highlights the impact of the $Ba_2TiSi_2O_8$ phase on bioactivity. Additionally, the carbonate peaks at 873 cm^{-1} and 1417 cm^{-1} to 1487 cm^{-1} confirmed the formation of CHA, critical for mimicking natural bone mineral.

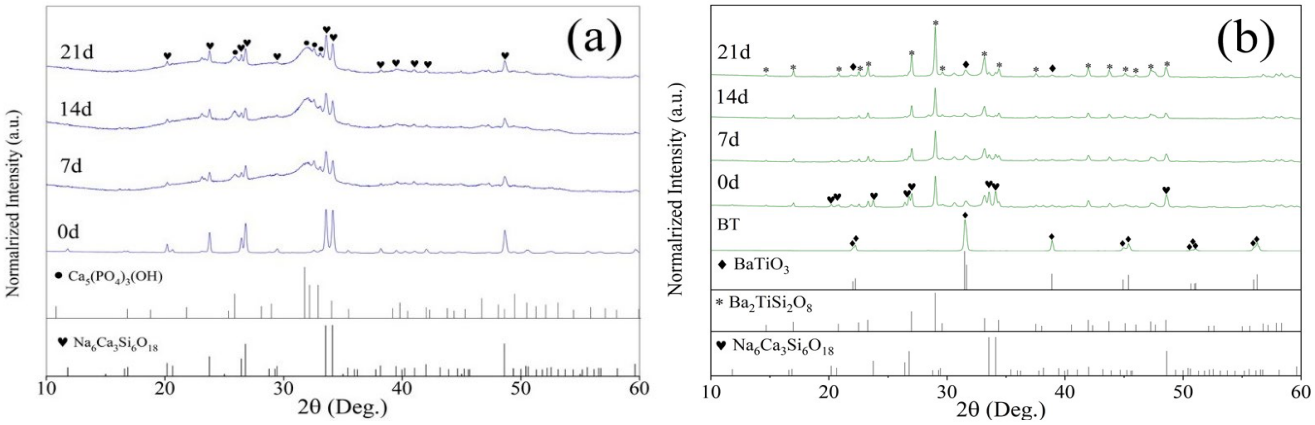

Figure 1. X-ray diffraction patterns in the 2θ range of 10° to 60° for the (a) 45S5, and (b) 45S5/BT25 composite scaffolds before and after 0 day, 7 days, 14 days, and 21 days immersion in SBF.

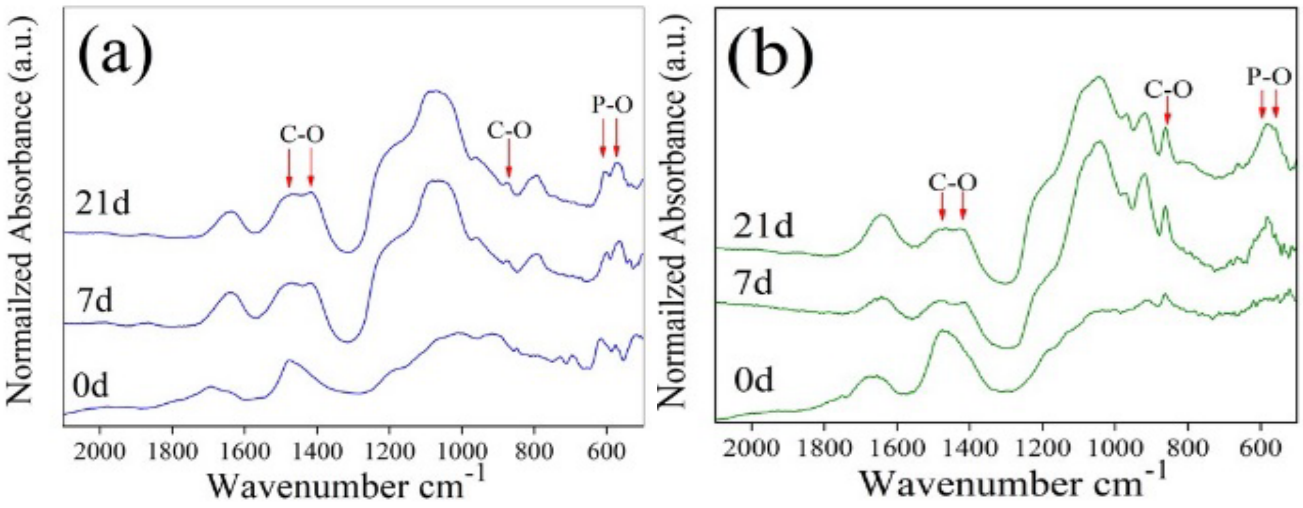

Figure 2. FTIR absorbance spectra for the (a) 45S5, and (b) 45S5/BT25 composite scaffolds before and after immersion in SBF.

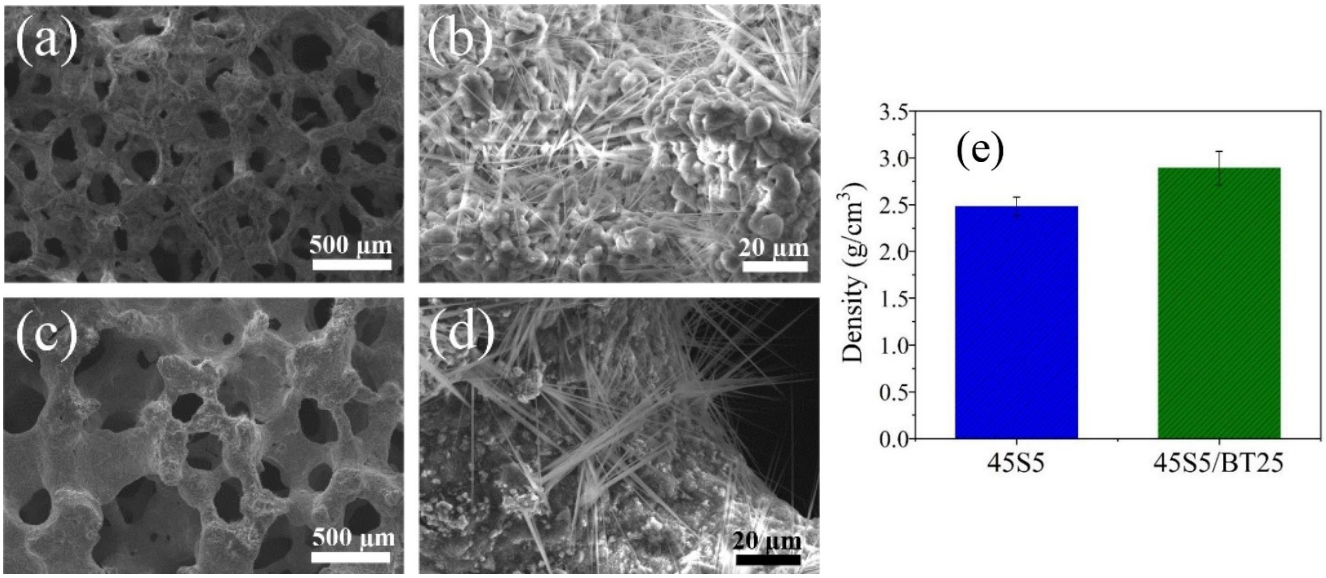

Figure 3. SEM image of 45S5 scaffolds (a) and (b), and 45S5/BT25 composite scaffolds (c) and (d) at different magnifications of 50 and 1000, and the density value before immersion in SBF solutions (e).

Figure 3(a-d) present SEM image of 45S5 and 45S5/BT25 scaffolds before immersion in SBF. Both 45S5 and 45S5/BT25 scaffolds exhibited a highly porous and interconnected structure. The average pore size of 45S5 and 45S5/BT25 scaffold were 471 ± 94 µm and 598 ± 58 µm, respectively, with average pore sizes resembling human bone (Figure 3(a,c). The increased pore size in the BT-modified scaffolds is attributed to the incorporation of larger BT particles. These pore sizes facilitate cell migration, nutrient diffusion, and vascularization, which are essential for bone regeneration. At higher magnifications (Figure 3(b,d), both compositions showed the presence of crystalline phase in needles form. This may be consistent with the structural isomorphic phase $CaO{\cdot}SiO_2$ [23]. The scaffold density increased significantly with BT addition, from 2.48 ± 0.10 $g{\cdot}cm^{-3}$ (45S5) to 2.89 ± 0.18 $g{\cdot}cm^{-3}$ (45S5/BT25) as seen in Figure 3(e). This is owing to BT has a relatively high density (~6.02 $g{\cdot}cm^{-3}$) compared to the 45S5 glass (~2.7 $g{\cdot}cm^{-3}$) [24,25]. The replacement of lower-density glassy components with higher-density $BaTiO_3$ particles directly increases the bulk density of the composite scaffold. The results of density measurements corresponded well with the SEM analysis.

The SEM images of 45S5 and 45S5/BT25 scaffolds after immersion in SBF at different times, are shown in Figure 4(a-l). At the early stage of immersion (7 days), the 45S5 scaffold exhibited cauliflower-shaped CHA crystals (Figure 4(a)), which were clearly visible under higher magnifications (Figure 4(b)). As the immersion time increased to 21 days, the CHA crystals on the 45S5 scaffolds showed improved homogeneity and coverage (Figure 4(c-f)), indicating progressive mineralization. In contrast, the 45S5/BT25 scaffolds showed no significant CHA formation at 7 days and 14 days of immersion as the formation of CHA crystals could not be clearly observed (Figure 4(g-j)). However, after 21 days of immersion, cauliflower-shaped CHA crystals began to appear (Figure 4(k-l)), though the coverage was less uniform compared to the 45S5 scaffolds. The correlation among XRD, FTIR, and SEM results demonstrates the delay in the formation of hydroxyapatite (HA), particularly CHA, on the 45S5/BT25 composite scaffolds.

XRD patterns indicated the presence of a stable $Ba_2TiSi_2O_8$ phase, which interferes with ion exchange and silica network dissolution, which are critical for CHA nucleation. The pH and weight loss of the scaffolds after immersion in SBF at different times can be seen in Table. It was found that the pH of the SBF solution increased throughout the immersion period, reflecting ongoing ionic exchange. For 45S5 scaffolds, the pH rose gradually from 8.02 to 8.06, while for 45S5/BT25 scaffolds, the increase was more rapid, from 7.69 to 7.86. This faster increase in pH for 45S5/BT25 scaffolds may be due to the presence of $Ba_2TiSi_2O_8$, which alters the ionic dynamics by releasing Ba and Ti ions into the solution. These ions could interact with the SBF, enhancing ion exchange and raising the pH more rapidly compared to 45S5 scaffolds, which primarily release Ca^{2+} and Na^+ ions. Additionally, the slower degradation of 45S5/BT25 scaffolds, due to the stabilizing effect of BT, likely contributes to a more controlled yet distinct increase in pH. Initially, the ionic exchange between the ions such as Ca^{2+} and Na^+ from 45S5 bioglass network and H^+ (or H_3O^+) from the SBF solution occurs, which leaves a poorly connected silica-rich layer [26,27]. This process results in an increase of the pH of the solution due to the increasing number of the OH^- ions that is dependent on the glass composition.

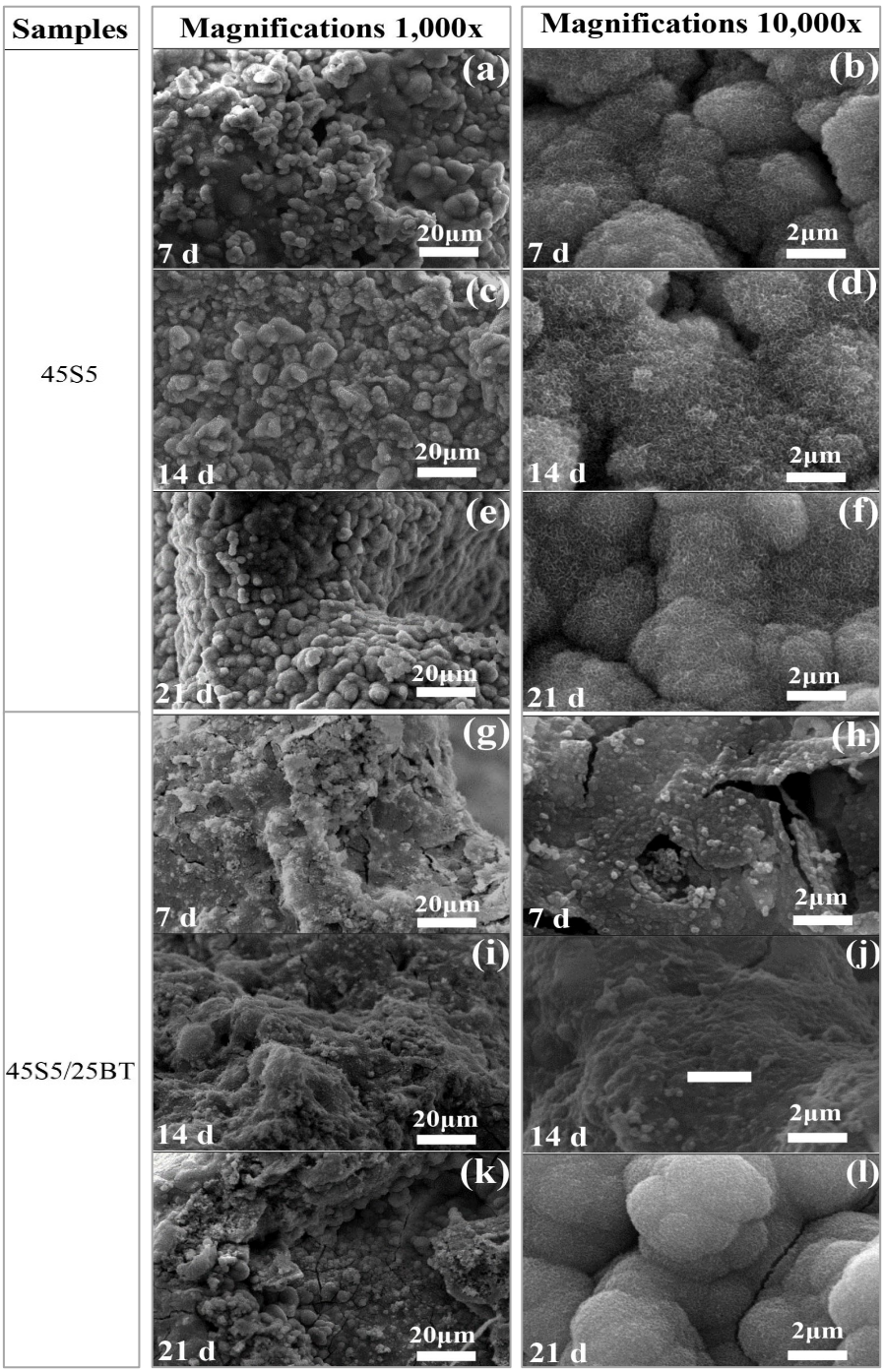

Figure 4. SEM image of 45S5 scaffolds after immersion in SBF for (a-b) 7 days, (c-d) 14 days, and (e-f) 21 days, and 45S5/BT25 composite scaffolds after immersion in SBF for (g-h) 7 days, (i-j) 14 days, and (k-l) 21 days, at different magnifications of 1000x and 10000x.

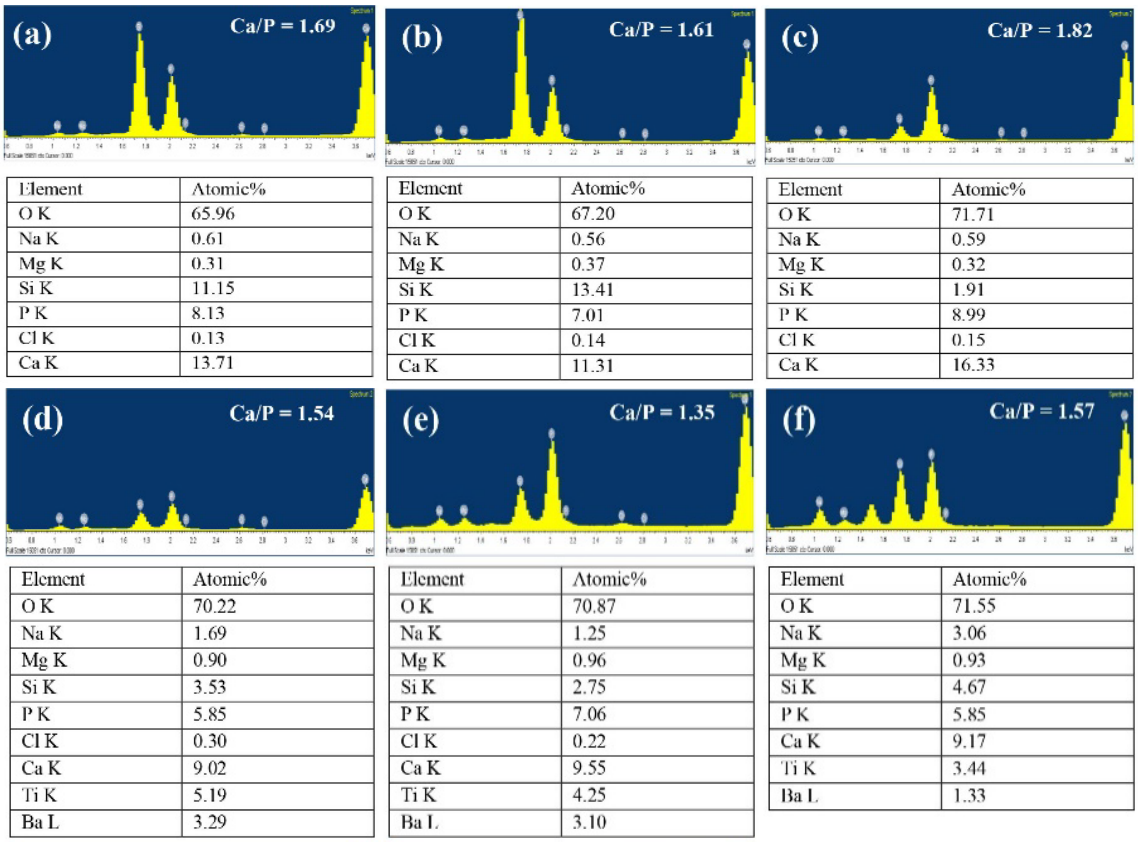

Element	Atomic%
O K	65.96
Na K	0.61
Mg K	0.31
Si K	11.15
P K	8.13
Cl K	0.13
Ca K	13.71

Element	Atomic%
O K	67.20
Na K	0.56
Mg K	0.37
Si K	13.41
P K	7.01
Cl K	0.14
Ca K	11.31

Element	Atomic%
O K	71.71
Na K	0.59
Mg K	0.32
Si K	1.91
P K	8.99
Cl K	0.15
Ca K	16.33

Element	Atomic%
O K	70.22
Na K	1.69
Mg K	0.90
Si K	3.53
P K	5.85
Cl K	0.30
Ca K	9.02
Ti K	5.19
Ba L	3.29

Element	Atomic%
O K	70.87
Na K	1.25
Mg K	0.96
Si K	2.75
P K	7.06
Cl K	0.22
Ca K	9.55
Ti K	4.25
Ba L	3.10

Element	Atomic%
O K	71.55
Na K	3.06
Mg K	0.93
Si K	4.67
P K	5.85
Ca K	9.17
Ti K	3.44
Ba L	1.33

Figure 5. EDS analysis of 45S5 scaffold after immersion in SBF for (a) 7 days, (b) 14 days, and (c) 21 days, and 45S5/BT25 scaffold after immersion in SBF for (d) 7 days, (e) 14 days and (f) 21 days.

Table 1. Characterization of 45S5 and 45S5/BT25 scaffolds after immersion in SBF at different times.

Samples	Dwell time	pH	Weight loss ± S.D. [%]
45S5	7 days	8.02	29 ± 0.66
	14 days	8.03	31 ± 3.81
	21 days	8.06	30 ± 1.32
45S5/BT25	7 days	7.69	19 ± 2.48
	14 days	7.83	22 ± 1.35
	21 days	7.86	21 ± 0.62

The atomic percentage of calcium (Ca) and phosphorus (P) was measured using EDS to inspect the Ca/P ratio (Figure 5(a-f)). The Ca/P ratio is essential to the formation of the CHA layer. The formation of CHA layer on the surface of biomaterials is a key indicator of bioactivity, particularly in applications involving bone repair and regeneration. CHA closely resembles the mineral component of natural bone. Theoretically, the Ca/P ratio should be approximately 1.67 for the formation of hydroxyapatite [28]. The lower Ca/P ratio of < 1.67, which indicates the formation of calcium-deficient apatite [29]. In contrast, the Ca/P ratio of > 1.76, which indicates the formation of a calcium-rich and much more stable apatite layer [30]. EDS data of 45S5 and 45S5/BT25 scaffold after immersion in SBF at different times are shown in Figure 5(a-f). The 45S5 scaffold showed the elements of O, Na, Mg, Si, P, Cl and Ca. For 45S5/BT25 scaffold, the elements of O, Na, Mg, Si, P, Cl, Ca, Ti and Ba were detected. The calcium-to-phosphorus (Ca/P) ratio of 45S5 scaffold obtained for the days 7 was 1.69 (Figure 5(a)). Further analysis of the days 14 and days 21 resulted in Ca/P rations of 1.61 and 1.82 respectively (Figure 5(b-c)). The obtained Ca/P ratios can be interpreted as CHA. For the 45S5/BT25 scaffold, the Ca/P ratios at days 7, 14, and 21 were 1.54, 1.35, and 1.57, respectively (Figure 5(d-f)). The decrease in the Ca/P ratio aligns with the insertion of Ba and Ti atoms into the structure of 45S5, which disrupts the bonding between Ca and phosphate (PO_4^{3-}) and delays HA crystallization. The degradation rates was evaluated by weight loss analysis after the scaffold was immersed in SBF. For the 45S5 scaffold, weight loss increases slightly from 29 ± 0.66% at 7 days to 31 ± 3.81% at 14 days, before slightly decreasing to 30 ± 1.32% at 21 days (Table 1). In contrast, the 45S5/BT25 scaffold exhibits lower weight loss, starting at 19 ± 2.48% at 7 days, increasing to 22 ± 1.35% at 14 days, and then slightly decreasing to 21 ± 0.62% at 21 days (Table 1). This behavior is attributed to the dense structure and reduced dissolution rate imparted by BT addition.

For biocompatibility studies, Ashutosh *et al.* [31] investigated the *in vivo* toxicity of HA-40 wt% $BaTiO_3$ particle eluates using a mouse model. Their initial *in vitro* evaluation showed that the eluates had no significant effect on cellular morphology, apart from a slight inhibition

likely caused by physical constraints. In our study, the crystalline powder of 45S5 bioactive glass doped with 25 wt% $BaTiO_3$ is expected to demonstrate low cytotoxicity, given its lower $BaTiO_3$ content and the inherently biocompatible nature of the 45S5 glass matrix. These findings suggest the potential of such composites for use in $BaTiO_3$-based piezoelectric implantable devices in biomedical applications.

The compressive strength of the scaffolds before immersion in SBF is shown in Figure 6. The 45S5/BT25 composite scaffold demonstrated a significantly higher compressive strength (2.0 ± 0.2 MPa) compared to the 45S5 scaffold (0.7 ± 0.1 MPa). Also, it was found that the compressive strength of the 45S5/BT25 scaffold was higher than the conventional 45S5 scaffold (1.2 ± 0.2 MPa), as reported by Baino *et al.* [32]. This phenomenon can be explained by the higher density of 45S5/BT25 composite scaffolds when compared to undoped 45S5 scaffolds (Figure 3(e)). The increase in strength can be attributed to the higher density and reinforcing effect of BT, which mitigates crack propagation within the composite. The compressive strength results of the fabricated composite scaffolds in this work are in the range of human trabecular bone (0.1 MPa to 16 MPa), making them suitable for load-bearing applications [33,34]. Compared to Polley *et al.* [11], who reported compressive strengths of 56.4 ± 7.6 MPa for 45S5/BT75 scaffolds, this is higher than the value observed in this study, possibly due to the higher BT addition volume. Despite this work obtaining lower compressive strengths, the interconnected porosity of the 45S5/BT25 scaffolds provides superior bioactivity, as evidenced by CHA formation. In terms of porosity, the 45S5/BT25 scaffolds outperform many conventional scaffolds due to their biomimetic pore structure. Moreover, the delayed CHA formation in 45S5/BT25 scaffolds could be advantageous in specific applications where controlled bioactivity is required to match the healing process. Bone healing occurs in distinct phases: inflammation, soft callus formation, hard callus formation, and remodeling. Rapid hydroxyapatite (HA) formation can lead to premature mineralization, creating a dense barrier that hinders cell infiltration and vascular ingrowth. In contrast, delayed bioactivity allows for gradual cell migration and matrix deposition before complete mineralization, enhancing scaffold integration. Controlled HA formation also enables sustained ion release (e.g., calcium, phosphate), which can promote osteogenesis and angiogenesis over time critical for large or slow-healing bone defects [35-37].

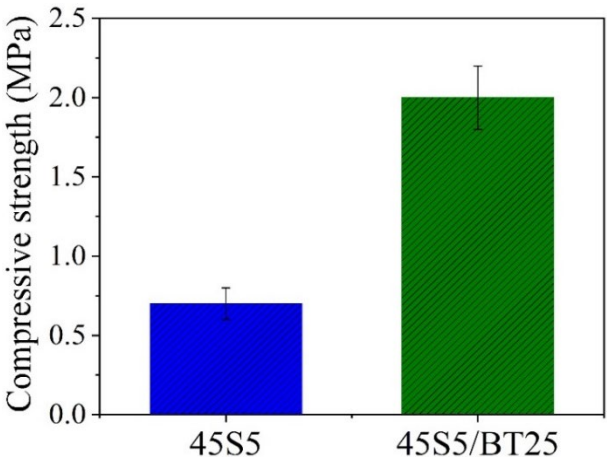

Figure 6. The compressive strength of 45S5 and 45S5/BT25 composite scaffold before soaking in SBF.

The trade-off between the mechanical properties of BT and the bioactivity of 45S5 bioactive glass arises from their distinct surface reaction behaviors in physiological environments. BT ceramic exhibited high mechanical strength and piezoelectric properties [10,11,38]. However, the ceramics cannot promote HA formation in SBF due to their chemically inert surface. In contrast, 45S5 bioactive glass readily undergoes surface reactions in SBF. Starting from ion exchange, silica dissolution, gel layer formation, and calcium-phosphate precipitation and culminating in the crystallization of HA, which makes it highly bioactive but mechanically fragile. When BT was incorporated into 45S5, the resulting composite exhibited a balance between improved mechanical strength and moderate bioactivity. Therefore, the integration of $BaTiO_3$ into 45S5 represents a strategic compromise, where mechanical reinforcement is achieved at the expense of some bioactive potential.

4. Conclusions

In this study, 45S5/BT25 composite scaffolds were successfully fabricated using foam replica technique. The incorporation of 25 wt% barium titanate (BT) into 45S5 bioglass resulted in highly porous scaffolds with average pore sizes of 471 ± 94 μm (45S5) and 598 ± 58 μm (45S5/BT25), closely resembling human bone. The addition of BT significantly improved scaffold density (2.89 ± 0.18 $g \cdot cm^{-3}$) and compressive strength (2.0 ± 0.2 MPa), making the material more suitable for load-bearing applications. Structural analysis confirmed the formation of a stable $Ba_2TiSi_2O_8$ crystalline phase, which contributed to a delayed carbonated hydroxyapatite (CHA) formation in BT-modified scaffolds. While CHA appeared on 45S5 after 7 days in SBF, it was only observed on 45S5/BT25 after 21 days. This controlled bioactivity may be advantageous for clinical applications requiring gradual mineralization, such as large bone defects or cases involving delayed healing.

Overall, the BT-modified 45S5 scaffolds present a promising balance between mechanical integrity and tunable bioactivity, supporting their potential use in personalized bone regeneration strategies. However, the delayed osteoconductivity may limit their use in applications requiring rapid integration. Future work will include comprehensive biocompatibility evaluation, beginning with *in vitro* assays such as cytotoxicity, cell proliferation, and osteogenic differentiation to confirm the material's safety and its ability to support bone tissue regeneration at the cellular level.

Acknowledgements

This work was financially supported by Thailand Science Research and Innovation (TSRI) and the Department of Science Service (DSS).

Reference

[1] F. Jianqing, Y. Huipin, and Z. Xingdong, "Promotion of osteogenesis by a piezoelectric biological ceramic," *Biomaterials*, vol. 18, pp. 1531–1534, 1997.

[2] R. Donate, R. Paz, R. Moriche, M. J. Sayagués, M. E. A. Domínguez, and M. Monzón, "An overview of polymeric composite scaffolds with piezoelectric properties for improved bone regeneration," *Materials & Design*, vol. 231, p. 112085, 2023.

[3] S. Shahi, S. Karbasi, T. Ahmadi, F. Naeimi, V. Goodarzi, and S. E. Barough, "Evaluation of physical, mechanical and biological properties of β-tri-calcium phosphate/Poly-3- hydroxybutyrate nano composite scaffold for bone tissue engineering application," *Advanced Performance Materials*, vol. 36. pp. 237–249, 2021.

[4] L. Siqueira, R. F. Gouveia, L. Grenho, F. J. Monteiro, M. H. Fernandes, and E. S. Trichês, "Highly porous 45S5 bioglass-derived glass-ceramic scaffolds by gelcasting of foams," *Journal of Materials Science*, vol. 53, pp. 10718–10731, 2018.

[5] L. L. Hench, and J. Wilson, *An introduction to bioceramics*, Advanced series in ceramic, World Scientific Singapore, 1993.

[6] D. Navarro da Rocha, L. de Andrade Gobbo, and M. Henrique Prado da Silva, "Production and characterization of niobate apatite," *Journal of Materials Research and Technology*, vol. 2, pp. 24–29, 2013.

[7] A. Kumar, S. Murugavel, A. Aditya, and A. R. Boccaccini, "Mesoporous 45S5 bioactive glass: Synthesis, in vitro dissolution and biominerlization behavior," *Journal of Materials Chemistry B*, vol. 44, pp. 1–44, 2017.

[8] L. L. Hench, "Chronology of bioactive glass development and clinical applications," *New Journal of Glass and Ceramics*, vol. 3, pp. 67–73, 2013.

[9] S. Midha, T. B. Kim, W. Bergh, P. D. Lee, J. R. Jones, and C. A. Mitchell, "Preconditioned 70S30C bioactive glass foams promote osteogenesis in vivo," *Acta Biomaterialia*, vol. 9, pp. 9169–9182, 2013.

[10] B. Saeidi, M. R. Derakhshandeh, M. D. Chermahini, and A. Doostmohammadi, "Novel porous barium titanate/nano-bioactive glass composite with high piezoelectric coefficient for bone regeneration applications," *Journal of Materials Engineering and Performance*, vol. 29, pp. 5420–5427, 2020.

[11] C. Polley, T. Distler, C. Scheufler, R. Detsch, H. Lund, A. Springer, D. Schneidereit, P. Friedrich, and A. R. Boccaccini, "3D printing of piezoelectric and bioactive barium titanate-bioactive glass scaffolds for bone tissue engineering," *Materials Today Bio*, vol. 21, p. 100719, 2023.

[12] H. Shokrollahi, F. Salimi, and A. Doostmohammadi, "The fabrication and characterization of barium titanate/akermanite nano-bio-ceramic with a suitable piezoelectric coefficient for bone defect recovery," *Journal of the Mechanical Behavior of Biomedical Materials*, vol. 74, pp. 365–370, 2017.

[13] A. S. Verma, D. Kumar, and A. K. Dubey, "Antibacterial and cellular response of piezoelectric $Na_{0.5}K_{0.5}NbO_3$ modified 1393 bioactive glass," *Materials Science and Engineering C*, vol. 116, p. 111138, 2020.

[14] A. K. Dubey, R. Kinoshita, and K. I. Kakimoto, "Piezoelectric sodium potassium niobate mediated improved polarization and in vitro bioactivity of hydroxyapatite," *Royal Society of Chemistry Advances*, vol. 5, p. 19638, 2015.

[15] J. Park, and R. S. Lakes, *Biomaterials: An Introduction*, Springer, Berlin, 2007.

[16] Y. Zhang, L. Chen, J. Zeng, K. Zhou, and D. Zhang, "Aligned porous barium titanate/hydroxyapatite composites with high piezoelectric coefficients for bone tissue engineering," *Materials Science and Engineering C*, vol. 39, pp. 143–149, 2014.

[17] Q. Fu, M. N. Rahaman, B. S. Bal, R. F. Brown, and D. E. Day, "Mechanical and in vitro performance of 13-93 bioactive glass scaffolds prepared by a polymer foam replication technique," *Acta Biomaterialia*, vol. 4, pp. 1854–1864, 2008.

[18] L. Stipniecen, I. Narkevica, M. Sokolova, J. Locs, and J. Ozolins, "Novel scaffolds based on hydroxyapatite/poly(vinyl alcohol) nanocomposite coated porous TiO_2 ceramics for bone tissue engineering," *Ceramics International*, vol. 42, pp. 1530–1537, 2016.

[19] L. Lefebvre, J. Chevalier, L. Gremillard, R. Zenati, G. Thollet, D. B. Assolant, and A. Govin, "Structural transformations of bioactive glass 45S5 with thermal treatments," *Acta Materialia*, vol. 55, pp. 3305–3313, 2007.

[20] B. R. Barrioni, A. C. Oliveira, M. D. F. Leite, and M. D. M. Pereira, "Sol-gel-derived manganese-releasing bioactive glass as a therapeutic approach for bone tissue engineering," *Journal of Materials Science*, vol. 52, pp. 8904–8927, 2017.

[21] Y. Zhu, and S. Kaskel, "Comparison of the in vitro bioactivity and drug release property of mesoporous bioactive glasses (MBGs) and bioactive glasses (BGs) scaffolds," *Microporous and Mesoporous Materials*, vol. 118, pp. 176–182, 2009.

[22] W. Li, H. Wang, Y. Ding, E. C. Scheithauer, O. M. Goudouri, A. Grünewalda, R. Detsch, S. Agarwal, and A. R. Boccaccini, "Antibacterial 45S5 Bioglass® -based scaffolds reinforced with genipin cross-linked gelatin for bone tissue engineering," *Journal of Materials Chemistry B*, vol. 3, pp. 3367–3378, 2015.

[23] D. Rohanová, A. R. Boccaccini, D. Horkavcová, P. Bozděchová, P. Bezdička, and M. Častorálová, "Is non-buffered DMEM solution a suitable medium for in vitro bioactivity tests?," *Journal of Materials Chemistry B*, vol. 2, pp. 5068–5076, 2014.

[24] A. Ehterami, M. Kazemi, B. Nazari, P. Saraeian, and M. Azami, "Fabrication and characterization of highly porous barium titanate based scaffold coated by Gel/HA nanocomposite with high piezoelectric coefficient for bone tissue engineering applications," *Journal of the Mechanical Behavior of Biomedical Materials*, vol. 79, pp. 195–202, 2018.

[25] D. G. Filip, V. A Surdu, A. V. Paduraru, and E. Andronescu, "Current development in biomaterials-hydroxyapatite and bioglass for applications in biomedical field: A Review," *Journal of Functional Biomaterials*, vol. 13, p. 248, 2022.

[26] S. Chajri, S. Bouhazma, I. Adouar, S. Herradi, M. Khaldi, B. El Bali, and M. Lachkar, "Synthesis, characterization and evaluation of bioactivity of glasses in the $CaO\text{-}SiO_2\text{-}P_2O_5\text{-}MgO$ system with different CaO/MgO ratios," *Journal of Physics*: *Conference Series*, vol. 1292, p. 012013, 2019.

[27] L. L. Fiench, and J. Wilson, "Surface-active biomaterials," *Science*, vol. 226, pp. 630–636, 1984.

[28] S. Ferraris, S. Yamaguchi, N. Barbani, M. Cazzola, C. Cristallini, M. Miola, E. Vernè, and S. Spriano, "Bioactive materials: In vitro investigation of different mechanisms of hydroxyapatite precipitation," *Acta Biomaterialia*, vol. 102, pp. 468–480, 2020.

[29] Z. LeGeros, "Properties of osteoconductive biomaterials: calcium phosphates," *Clinical Orthopaedics and Related Research*, vol. 395, pp. 81–98, 2002.

[30] P. K. Chakraborty, J. Adhikari, and P. Saha, "Variation of the properties of sol-gel synthesized bioactive glass 45S5 in organic and inorganic acid catalysts," *Materials Advances*, vol. 2, pp. 413–425, 2021.

[31] A. K. Dubey, G. Thrivikraman, and B. Basu, "Absence of systemic toxicity in mouse model towards $BaTiO_3$ nanoparticulate based eluate treatment," *Journal of Materials Science: Materials in Medicine*, vol. 26, p. 103, 2015.

[32] F. Baino, and E. Fiume, "Mechanical characterization of 45S5 bioactive glass-derived scaffolds," *Materials Letters*, vol. 245, pp. 14–17, 2019.

[33] L. C. Gerhardt, and A. R. Boccaccini, "Bioactive glass and glass-ceramic scaffolds for bone tissue engineering," *Materials*, vol. 3, pp. 3867–3910, 2010.

[34] T. M. Keaveny, E. F. Morgan, G. L. Niebur, and O. C. Yeh, "Biomechanics of trabecular bone," *Annual Review of Biomedical Engineering*, vol. 3, pp. 307–333, 2001.

[35] T. A. Einhorn, and L. C. Gerstenfeld, "Fracture healing: Mechanisms and interventions," *Nature Reviews Rheumatology*, vol. 11, pp. 45–54, 2015.

[36] A. N. Nomm, L. Hupa, D. Rohanová, and D. S. Brauer, "A review of acellular immersion tests on bioactive glasses-influence of medium on ion release and apatite formation," *International Journal of Applied Glass Science*, vol. 11, pp. 537–551, 2020.

[37] Y. Tang, C. Wu, Z. Wu, L. Hu, W. Zhang, and K. Zhao, "Fabrication and in vitro biological properties of piezoelectric bioceramics for bone regeneration," *Scientific Reports*, vol. 7, p. 43360, 2017.

[38] H. Huang, K. Wang, X. Liu, X. Liu, J. Wang, M. Suo, H. Wang, S. Chen, X. Chen. and Z. Li, "Piezoelectric biomaterials for providing electrical stimulation in bone tissue engineering: Barium titanate," *Journal of Orthopaedic Translation*, vol. 51, pp. 94–107, 2025.